IEEE Access
Multidisciplinary | Rapid Review | Open Access Journal

Received January 14, 2020, accepted February 2, 2020, date of publication February 12, 2020, date of current version February 26, 2020.

Digital Object Identifier 10.1109/ACCESS.2020.2973501

Design of Space-Frequency Index Modulation Waveforms for MIMO–OFDM Heterogeneous Networks

RUI CAO, XIA LEI, YUE XIAO, (Member, IEEE), AND YOU LI
National Key Laboratory of Science and Technology on Communications, University of Electronic Science and Technology of China, Chengdu 611731, China
Corresponding author: Xia Lei (leixia@uestc.edu.cn)

This work was supported in part by the National Science Foundation of China under Grant 61771106, in part by the National Key Research and Development Program of China under Grant 2018YFC0807101, and in part by the Science and Technology Department of Sichuan Province under Grant 2018GZ0092.

ABSTRACT In this paper, a novel framework to efficiently design the waveforms toward heterogeneous networks (HetNets) is proposed. The proposed scheme combines the index modulation (IM) concept with multiple-input multiple-output (MIMO) and orthogonal frequency-division multiplexing (OFDM) techniques and jointly considers the resources on both spatial and frequency domains to optimize the transmission signals. Furthermore, a generalized union bound expression is derived first to disclose the potential diversity gain for the spatial-frequency index modulation (SFIM) system and based on the developed bound different impacts of activating spatial and frequency domains resources for transmission are analyzed. Following the theoretical insights, two novel transmit schemes, termed as enhanced SFIM with non-overlap (ESFIM-NO) and enhanced SFIM with overlap (ESFIM-O), toward higher diversity gains are proposed. We show that the proposed methods can significantly improve the diversity of both index and amplitude phase modulation (APM) domains for achieving higher reliability for the entire HetNets. Finally, the simulation results are given to verify the theoretical analysis and system error performance.

INDEX TERMS Multi-dimensional index modulation, coding gains, diversity gains.

I. INTRODUCTION

The heterogeneous networks (HetNets) have emerged as a promising solution to support high data rate and a variety of services required by future wireless communication networks by enabling the terminals be capable of processing signals transmitted from both macrocell and small cell [1]–[6]. However, the cross-tier interferences induced by the overlaid architecture pose a significant challenge for HetNets [7]–[10]. Recently, non-orthogonal multiple access (NOMA) techniques were developed to help HetNets manage the interferences [11]–[13]. Moreover, the unique feature of index modulation (IM) also makes it a candidate waveform for the signals of one tier in HetNets to control the interferences [14]. Therefore, a novel framework to design the waveforms for IM aided multiple-input multiple-output (MIMO)-orthogonal frequency-division multiplexing (OFDM) systems is proposed in this paper to further enhance the reliability of the tier signals.

The generalized IM technology differs from conventional transmission schemes, where the information bits are conveyed only by amplitude phase modulation (APM) signals chosen from a fixed constellation [15]–[18]. In contrast, besides APM signals, IM systems exploit the indices of various transmission units to convey information bits implicitly. Thanks to the researchers' efforts, so far, a large variety of indices can be utilized for IM systems, such as the indices of transmit/receive antennas [19], subcarriers [20], time slots [21], and so on. Since the inactivated transmission units can convey information bits without energy consumption, the index modulation is regarded as a promising technology for the future wireless networks including HetNets [22].

Categorized in the family of IM technology, the spatial modulation (SM), which uses the indices of antennas to convey additional information bits, is well-known for its high spectral and energy efficiency with low complexity of

The associate editor coordinating the review of this manuscript and approving it for publication was Qilian Liang.

transmitter design. Interested reader are referred to [23], [24] to have a comprehensive view of the achievements with regard to SM.

Inspired by SM, the concept of IM is extended to the OFDM system recently, where the indices of subcarriers are used to convey additional information bits. Similar to SM, various schemes are introduced to improve the system performances. More specifically, the authors of [25] proposed the design of interleaving for subcarriers with better bit error rate (BER) performance by making the fadings in a block uncorrelated. Moreover, in [26], a novel transmission scheme, termed as coordinate interleaved OFDM-IM (CI-OFDM-IM) is proposed by selecting two groups of subcarriers independently to convey the I and Q branches of APM signals, respectively. Therefore, the transmit diversity gains can be obtained for CI-OFDM-IM. Also aiming to increase the transmit diversity order, in [27], the authors proposed to utilize the APM signals chosen from multiple constellations to bear the same information bits. Furthermore, in [28], the authors leveraged the repeated coding to propose a novel scheme, termed as repeated MCIK-OFDM (ReMO), to increase the transmit diversity order. However, the transmit diversity orders of APM signals and index part are not matched in ReMO. The index part can only achieve a diversity order of two, which limits the whole system error performance.

For exploiting the potential of IM further, some researchers are studying to combine OFDM with index modulation (OFDM-IM) with the MIMO technology to take advantages from both sides. More specifically, in [29], the concept of OFDM-IM has been extended to multiple antennas for achieving higher spectral efficiency. The proposed system is defined as MIMO-OFDM-IM and it is reported that significant SNR gains can be obtained by the MIMO-OFDM-IM system compared with the conventional MIMO-OFDM system. It is worthy to note that each antenna in the MIMO-OFDM-IM system activates the subcarrier independently, which limits the number of available index patterns. In order to solve this limitation, in [30], the authors proposed two spatial-frequency joint index modulation schemes, termed as generalized joint space-frequency index modulation (G-JSFIM) and Kronecker product-based joint space-frequency index modulation (KP-JSFIM). The simulation results showed that G-JSFIM can achieve the same error performance as MIMO-OFDM-IM with higher spectrum efficiency, while KP-JSFIM can provide the best error performance for low spectrum efficiency (SE) scenarios. Similar to KP-JSFIM, the authors of [31] also considered to jointly use spatial-frequency resource units to generate waveforms, however, antenna selection is carried out before index modulation to reduce the number of required radio frequency links. In [32] and [33], the performances of the SFBC-OFDM system are evaluated with channel estimation error and TWDP Fading Channel, respectively. Moreover, the index modulation concept has also been combined with compressed sensing technique in [34] to reduce the complexity of the receiver. For relay systems, a novel scheme was proposed in [35] to reduce the overhead while improving the error performance. A novel amplify-and-forward relay-assisted OFDM-IM system was proposed in [36] to reduce the system delay and energy consumption.

In this paper, a systematic waveform design to achieve enhanced transmit diversity for one tier of HetNets is proposed and the contributions of this paper are summarized as follows. Two novel transmit pattern generation schemes, termed as ESFIM-NO and ESFIM-O, are proposed. Specifically, ESFIM-O achieves higher order of transmit diversity at the same spectral efficiency compared to ESFIM-NO, while ESFIM-NO outperforms ESFIM-O at low SNR region due to larger minimum Euclidean distance. The difference to current SFIM systems lies in that we focus on enhancing the transmit diversity order by designing the transmit patterns. Unlike other current SFIM systems where a group of subcarriers are mapped with different IQ symbols, the proposed system actives multiple subcarriers to convey the same IQ symbol and the positions of active subcarriers are carefully designed. The theoretical and simulation results show that the proposed schemes obtain higher order of transmit diversity compared to existing SFIM systems without increasing the number of transmit antennas. Moreover, a generalized union bound expression for analyzing the transmit diversity orders of the SFIM system is derived.

The remainder of this paper is organized as follows. In Section II, the system model is presented. In Section III, two novel waveform design methods are proposed. In Section IV, the numerical results are given to verify the analysis and system performance. Finally, the conclusion is given in Section V.

Notations: $\mathbf{a}$ and $\mathbf{A}$ denote a vector and a matrix, respectively. $\odot$ is the Hadamard product and $\bigcup$ is the union operator for sets. $\otimes$ is the Kronecker product. $\lfloor\rfloor$ is the floor operator. $\mathbf{A}_{:,i}$ and $\mathbf{A}_{j,:}$ represent the ith column and jth row of the matrix $\mathbf{A}$, respectively.

II. SYSTEM MODEL

Consider a system equipped with N_t transmit and N_r receive antennas and each antenna transmits OFDM signals with an IFFT length of N. Hence, there are $N_t \times N$ space-frequency resource units available for each OFDM symbol period and the architecture of the transmitter is shown in Fig. 1. Assuming M information bits are conveyed during each OFDM symbol time, the coming bits are partitioned into G groups with $m = M/G$ bits for each group. Accordingly, the spatial-frequency resources are divided into G groups and $n = N_t \times n_b$ units are responsible for the transmission of the m bits, where n_b is the number of subcarriers selected from each transmit antenna. Without loss of generality, we only consider the first space-frequency group in the following parts of this paper.

For the first group, m information bits are further divided into two parts, containing m_1 and m_2 information bits, respectively, i.e., $m = m_1 + m_2$. The m_1 information bits are utilized to select a specific transmit pattern, which activates only

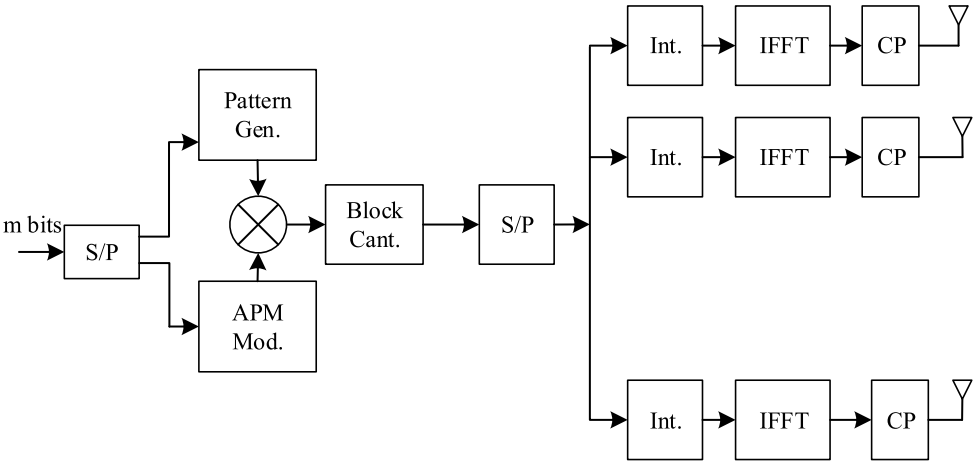

FIGURE 1. Transmitter architecture of generalized spatial-frequency index modulation systems.

part of available resource units while keeping the remaining silent. Assuming the group has k active resource units, $m_1 = \lfloor \log_2(C(n,k)) \rfloor$ bits can be mapped into the index domain. The remaining m_2 bits are conveyed by the conventional APM signals chosen from an $\mathcal{M}$-ary constellation $\mathcal{Q}$. After information mapping, G groups are concatenated and distributed to N_t antennas. On each antenna, normalized IFFT operations are applied after interleaving. Then, the waveform for transmission is formed by adding the cyclic prefix with the length of h_{cp}.

The waveforms are sent via a frequency selective Rayleigh fading MIMO channel. Denote $\mathbf{q}_t^r \in \mathbb{C}^{L_h \times 1}$ as the L-tap channel fading from the tth transmit antenna to the rth receive antenna in the time domain, whose elements are i.i.d Rayleigh random variables obeying $\mathcal{CN}(0, \frac{1}{L_h})$. The corresponding frequency domain fading coefficients from the tth transmit antenna to the rth receive antenna for the first group can be represented as $\mathbf{h}_t^r = [h_{t,1}^r, \dots h_{t,a}^r \cdots h_{t,n_b}^r]^T$, where $h_{t,a}^r \in \mathbb{C}$ is the channel fading coefficient on the ath subcarrier. Thus, for the first group, the coefficient matrix related to the rth receive antenna can be given as $\mathbf{H}^r = [\mathbf{h}_1^r, \mathbf{h}_2^r \cdots \mathbf{h}_{N_t}^r]$ and the entire channel coefficients in the frequency domain are given as $\mathbf{H} = [(\mathbf{H}^1)^T, (\mathbf{H}^2)^T \cdots (\mathbf{H}^{N_r})^T]^T$.

Assuming the ith, $i = 1, \cdots 2^m$, legitimate space-frequency index modulation symbol is selected, the transmit signals on the tth antenna can be presented as $\mathbf{s}_t^i = [s_{t,1}^i, s_{t,2}^i \cdots s_{t,n_b}^i]^T$, where $s_{t,a}^i \in \tilde{\mathcal{Q}} = \{0, \mathcal{Q}\}$, $a = 1, 2 \cdots n_b$. Thus, the signal matrix for entire N_t antennas can be denoted as $\mathbf{S}^i = [\mathbf{s}_1^i, \mathbf{s}_2^i \cdots \mathbf{s}_{N_t}^i]$. Therefore, the received signal $\mathbf{y}_r \in \mathbb{C}^{n_b \times 1}$ in the frequency domain on the rth receive antenna for the first group can be represented as

$$\mathbf{y}_r = \sqrt{\rho} \sum_{t=1}^{N_t} \mathbf{H}_{:,t}^r \odot \mathbf{S}_{:,t}^i + \mathbf{n}_r, \tag{1}$$

where $\rho = n/k$ is the normalization factor, each element in $\mathbf{n}_r \in \mathbb{C}^{n_b \times 1}$ is additive white Gaussian noise (AWGN) in the frequency domain and obeys $\mathcal{CN}(0, N_0)$. Therefore, after maximum likelihood (ML) detection, the estimate of the signal can be expressed as

$$\hat{i} = \underset{i}{\operatorname{argmin}} \sum_{r=1}^{N_r} \left\| \mathbf{y}_r - \sqrt{\rho} \sum_{t=1}^{N_t} \mathbf{H}_{:,t}^r \odot \mathbf{S}_{:,t}^i \right\|^2. \tag{2}$$

III. DIVERSITY ANALYSIS AND WAVEFORM DESIGN

In this section, a novel expression for the diversity of spatial-frequency index modulation (SFIM) is derived first, which offers an insight for the impacts of using spatial and frequency units for the diversity gains of IM. Based on the insights, two novel waveform designs, termed as enhanced SFIM with non-overlap (ESFIM-NO) and enhanced SFIM with overlap (ESFIM-O), are proposed to enhance the transmit diversity gain, which can be used for the signals of one tier in HetNets to enhance the reliability of the entire system.

A. DIVERSITY ANALYSIS FOR SFIM SYSTEMS

In order to analyze and compare all the SFIM schemes under the same framework, SFIM is regarded as selecting a block-wise signal $\mathbf{S}^i$ from an index modulation constellation whose elements are in $\tilde{\mathcal{Q}}$. Therefore, the transmit signal for the first group can be shown in Fig. 2, where $n_b \times N_t$ basic resource units are available for the first group.

With the ML detection, the conditional probability of the pairwise error in the case where $\mathbf{S}^j$ is detected when $\mathbf{S}^i$ is sent can be represented as (3), as shown at the bottom of the next page.

Using the Q-function, the instantaneous pairwise error probability (PEP) can be represented as

$$P(i \to j|\mathbf{H}) = Q\left(\sqrt{\frac{\sum_{r=1}^{N_r} \left\| \sum_{t=1}^{N_t} \sqrt{\rho} \mathbf{H}_{:,t}^r \odot (\mathbf{S}_{:,t}^i - \mathbf{S}_{:,t}^j) \right\|^2}{2N_0}}\right), \tag{4}$$

where $Q(x) = \frac{1}{2\pi} \int_x^\infty \exp(-\frac{t^2}{2})$ is the Gaussian tail probability [28]. By using the approximation

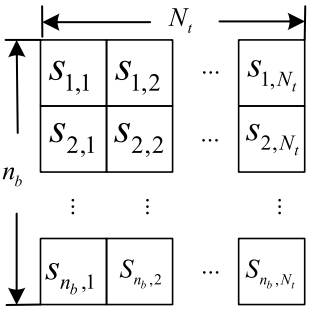

FIGURE 2. The generalized spatial-frequency transmit block for the first group.

$Q(x) \approx \frac{1}{12}e^{-x^2/2} + \frac{1}{4}e^{-2x^2/3}$, the instantaneous PEP can be approximated as

$$P(i \to j|\mathbf{H}) \approx \frac{1}{12} e^{-\frac{\sum_{r=1}^{N_r} \left\| \sum_{t=1}^{N_t} \sqrt{\rho}\mathbf{H}^r_{:,t} \odot (\mathbf{S}^i_{:,t} - \mathbf{S}^j_{:,t}) \right\|^2}{4N_0}} + \frac{1}{4} e^{-\frac{\sum_{r=1}^{N_r} \left\| \sum_{t=1}^{N_t} \sqrt{\rho}\mathbf{H}^r_{:,t} \odot (\mathbf{S}^i_{:,t} - \mathbf{S}^j_{:,t}) \right\|^2}{3N_0}}. \quad (5)$$

Applying the moment generating functions (MGF) method, the unconditional PEP can be attained as

$$P(i \to j) \approx \frac{1}{12} T_1 + \frac{1}{4} T_2 \quad (6)$$

where

$$T_1 = \prod_{a=1}^{n_b} \left(1 + \frac{\rho}{4N_0} \left\| \mathbf{S}^i_{a,:} - \mathbf{S}^j_{a,:} \right\|^2\right)^{-N_r I(\mathbf{S}^i_{a,:}, \mathbf{S}^j_{a,:})}, \quad (7)$$

$$T_2 = \prod_{a=1}^{n_b} \left(1 + \frac{\rho}{3N_0} \left\| \mathbf{S}^i_{a,:} - \mathbf{S}^j_{a,:} \right\|^2\right)^{-N_r I(\mathbf{S}^i_{a,:}, \mathbf{S}^j_{a,:})}, \quad (8)$$

$$I(\mathbf{x}, \mathbf{y}) = \begin{cases} 1 & \mathbf{x} \neq \mathbf{y} \\ 0 & \text{else.} \end{cases} \quad (9)$$

Note that, for a PEP, the signals on a subcarrier can contribute to the transmit diversity if and only if there is an error between the transmitted signal and incorrectly detected one on this subcarrier, i.e., $\mathbf{S}^i_{a,:} \neq \mathbf{S}^j_{a,:}$. The signals on different transmit antennas with the same subcarrier index can only determine the coding gain. Thus, the transmit diversity order corresponding to the PEP $P(i \to j)$ can be calculated as

$$\Phi(i, j) = \sum_{a=1}^{n_b} I(\mathbf{S}^i_{a,:}, \mathbf{S}^j_{a,:}). \quad (10)$$

Therefore, the transmit diversity order for the entire system can be represented as

$$D = \min_{i,j} \Phi(i, j) = \min(D_I, D_M). \quad (11)$$

where D_I and D_M are the transmit diversity order of the index and APM signal domains, respectively, and the analytic upper bounds of the symbol error rate and BER can be expressed as

$$P_s = \frac{1}{2^m} \sum_i \sum_{j \neq i} P(i \to j), \quad (12)$$

$$P_b = \frac{1}{m2^m} \sum_i \sum_{j \neq i} \text{Ham}(i, j) P(i \to j), \quad (13)$$

where $\text{Ham}(i, j)$ is the hamming distance.

B. WAVEFORM DESIGN

Inspired by the results in Sec. III-A, we propose two novel waveform designs, termed as ESFIM-NO and ESFIM-O by binding the basic resource units into blocks and the basic resource units in a block are mapped with the same APM symbol. The indices of the constructed blocks and the APM symbols mapped to the blocks are named as virtual indice and virtual APM symbols in order to distinguish from the conventional SFIM systems. By sophistically binding, the transmit diversity of the both virtual index and virtual APM symbol can be increased, which leads to the improvement of the error performance for the entire system.

It should be emphasized that the proposed scheme in [28] modulated multiple active subcarriers with the same APM symbol as well. However, it can only increase the transmit diversity order of the APM symbol but the transmit diversity order of the index domain is still limited to two, leading the transmit diversity order of the entire system to be two. In contrast, our approaches can improve the transmit diversity

$$\begin{aligned} &P(i \to j|\mathbf{H}) \\ &= P\Big(\sum_{r=1}^{N_r} \Big\| \mathbf{y}_r - \sqrt{\rho} \sum_{t=1}^{N_t} \mathbf{H}^r_{:,t} \odot \mathbf{S}^i_{:,t} \Big\|^2 > \sum_{r=1}^{N_r} \Big\| \mathbf{y}_r - \sqrt{\rho} \sum_{t=1}^{N_t} \mathbf{H}^r_{:,t} \odot \mathbf{S}^j_{:,t} \Big\|^2 \Big) \\ &= P\Big(\sum_{r=1}^{N_r} \|\mathbf{n}_r\|^2 > \sum_{r=1}^{N_r} \Big\| \sqrt{\rho} \sum_{t=1}^{N_t} \mathbf{H}^r_{:,t} \odot \mathbf{S}^i_{:,t} - \sqrt{\rho} \sum_{t=1}^{N_t} \mathbf{H}^r_{:,t} \odot \mathbf{S}^j_{:,t} \Big\|^2 \Big) \\ &= P\Big(\sum_{r=1}^{N_r} 2\sqrt{\rho} \Re \Big[\Big(\sum_{t=1}^{N_t} \mathbf{H}^r_{:,t} \odot \mathbf{S}^j_{:,t} - \sum_{t=1}^{N_t} \mathbf{H}^r_{:,t} \odot \mathbf{S}^i_{:,t} \Big)^H \mathbf{n}_r \Big] > \sum_{r=1}^{N_r} \Big\| \sqrt{\rho} \sum_{t=1}^{N_t} \mathbf{H}^r_{:,t} \odot \mathbf{S}^i_{:,t} - \sqrt{\rho} \sum_{t=1}^{N_t} \mathbf{H}^r_{:,t} \odot \mathbf{S}^j_{:,t} \Big\|^2 \Big) \end{aligned} \quad (3)$$

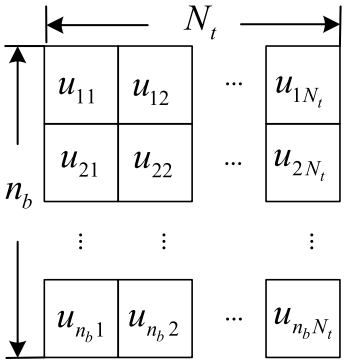

FIGURE 3. Representation of the resource units in the first group.

order of both the virtual index and virtual APM symbol simultaneously.

Denote u_{at} as the basic resource unit provided by the ath subcarrier on the tth transmit antenna. Then, the resource units in the first group can be illustrated in Fig. 3. In the following sections, two situations are considered according to whether the different virtual blocks contain the same basic resource units.

1) BINDING RESOURCE UNITS WITH NON-OVERLAP

In this section, the binding with non-overlapping basic resource units is considered. Without loss of generality, we still consider the first group, which contains $n_b \times N_t$ space-frequency resource units. All the units in the first group can be represented as a matrix $\mathbf{U}$, where u_{at} is its element, i.e., $\mathbf{U}_{a,t} = u_{at}$. By binding d units without overlapping, the virtual blocks after binding can be given as $\mathbf{W} = \{\mathbf{w}_{ct}\}$, where

$$\mathbf{w}_{ct} = \begin{Bmatrix} \mathbf{U}_{((c-1)\times d+1),t} \\ \mathbf{U}_{((c-1)\times d+2),t} \\ \vdots \\ \mathbf{U}_{((c-1)\times d+d),t} \end{Bmatrix} \tag{14}$$

represents the cth virtual block on the tth transmit antenna. Therefore, the binding with non-overlap means that

$$\mathbf{w}_{ct} \cap \mathbf{w}_{c't'} = \emptyset \qquad c \neq c' \text{ and } t \neq t'.$$

Let n_v and K_v represent the number of virtual blocks and the active ones, respectively, the number of virtual index patterns is $V = 2^{\lfloor \log_2 C(n_v, K_v) \rfloor}$.

In order to illustrate the method of binding with non-overlap more clearly, a specific example is given as follow, where $N_t = 2, n_b = 4, d = 2$. The binding strategy is shown in Fig. 4, where the basic resource units with the same colour belong to the same virtual block and each virtual block can be expressed as

$$\begin{aligned} \mathbf{w}_{11} &= \{u_{11}, u_{21}\} \\ \mathbf{w}_{21} &= \{u_{31}, u_{41}\} \\ \mathbf{w}_{12} &= \{u_{12}, u_{22}\} \\ \mathbf{w}_{22} &= \{u_{32}, u_{42}\}. \end{aligned} \tag{15}$$

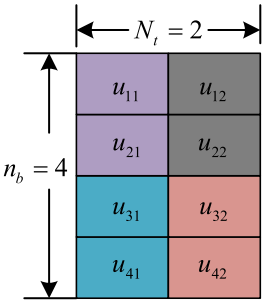

FIGURE 4. The binding with non-overlap for the first group with $d = 2$.

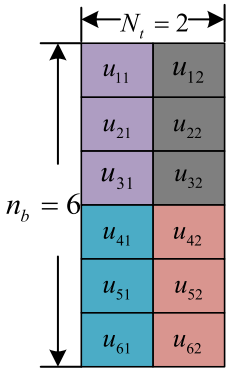

FIGURE 5. The binding with non-overlap for the first group with $d = 3$.

If higher transmit diversity order is required by using the binding with non-overlap, the group with larger number of basic resource units are needed. In Fig. 5, a binding with $d = 3$ is presented, where each virtual block can be expressed as

$$\begin{aligned} \mathbf{w}_{11} &= \{u_{11}, u_{21}, u_{31}\} \\ \mathbf{w}_{21} &= \{u_{41}, u_{51}, u_{61}\} \\ \mathbf{w}_{12} &= \{u_{12}, u_{22}, u_{32}\} \\ \mathbf{w}_{22} &= \{u_{42}, u_{52}, u_{62}\}. \end{aligned} \tag{16}$$

Obviously, there is a SE cost for pursuing higher error performance if using the binding with non-overlap.

For evaluating the error performance of the scheme, we category the error events into two types: the virtual block index errors and virtual APM symbol errors. Moreover, denote $\Psi^i = \{v_1^i, v_2^i \ldots v_{K_v}^i\}$ the index set of the active virtual blocks of the transmitted signal while $\Psi^j = \{v_1^j, v_2^j \ldots v_{K_v}^j\}$ as the detected index set of the active virtual blocks and $v_k^i, v_k^j \in \{1, 2, \ldots, N_t n_b/d\}$. Then, only the PEP $P(\Psi^i \to \Psi^j)\, j \in \Lambda_i$ satisfying $|\Psi^i - \Phi_{ij}| = 1$ is considered for virtual index errors, where $\Phi_{ij} = \Psi^i \cap \Psi^j$. Then, the virtual index error rate (VIER) can be approximated as

$$P_V \approx \frac{1}{V} \sum_{i=1}^{V} \sum_{j \in \Lambda_i} P(\Psi^i \to \Psi^j). \tag{17}$$

Denoting $\tilde{v}^i = \Psi^i - \Phi_{ij}$ and $\tilde{v}^j = \Psi^j - \Phi_{ij}$, the basic resource units in the virtual blocks corresponding to

the indice $\tilde{v}^i$ and $\tilde{v}^j$ can be represented as $\{\tilde{u}^i_{at}\}$ and $\{\tilde{u}^j_{a't'}\}$, respectively. These units can be further divided into two sets, where

$$\Omega^s_{ij} = \{\tilde{u}^i_{at}, \tilde{u}^j_{a't'}\} \tag{18}$$

contains the units with the same subcarrier index but different antenna indices, i.e., $a = a', t \neq t'$ and

$$\Omega^d_{ij} = \{\tilde{u}^i_{at}\} \cup \{\tilde{u}^j_{a't'}\} - \Omega^s_{ij} \tag{19}$$

contains the units with different subcarrier indice, i.e., $a \neq a'$.

Denoting $\mathbf{H}^r\left\langle\tilde{u}^i_{at}\right\rangle$ as the channel coefficient on the ath subcarrier from the tth transmit to the rth receive antenna, the instantaneous PEP with $j \in \Lambda_i$ can be given as

$$P(\Psi^i \to \Psi^j|\mathbf{H}) = Q(\sqrt{\frac{T^d_i + T^d_j + T^s_{ij}}{2N_0}}) \tag{20}$$

where

$$T^d_i = \sum_{r=1}^{N_r} \sum_{\tilde{u}^i_{at} \in \Omega^d_{ij}} \rho \left\|\mathbf{H}^r\left\langle\tilde{u}^i_{at}\right\rangle\right\|^2, \tag{21}$$

$$T^d_j = \sum_{r=1}^{N_r} \sum_{\tilde{u}^j_{a't'} \in \Omega^d_{ij}} \rho \left\|\mathbf{H}^r\left\langle\tilde{u}^j_{a't'}\right\rangle\right\|^2, \tag{22}$$

$$T^s_{ij} = \sum_{r=1}^{N_r} \sum_{a} \rho \left\|\mathbf{H}^r\left\langle\tilde{u}^i_{at}\right\rangle - \mathbf{H}^r\left\langle\tilde{u}^j_{at'}\right\rangle\right\|^2, \tag{23}$$

where $u^i_{at}, u^j_{at'} \in \Omega^s_{ij}$.

By using the Q function approximation, we can obtain

$$P(\Psi^i \to \Psi^j|\mathbf{H}) \approx \frac{1}{12}C_1 + \frac{1}{4}C_2. \tag{24}$$

where

$$C_1 = e^{-\frac{T^d_i + T^d_j + T^s_{ij}}{4N_0}}, \tag{25}$$

$$C_2 = e^{-\frac{T^d_i + T^d_j + T^s_{ij}}{3N_0}}. \tag{26}$$

Then, the unconditional PEP can be expressed as

$$P(\Psi^i \to \Psi^j) \approx \frac{1}{12}\mathrm{E}[C_1] + \frac{1}{4}\mathrm{E}[C_2]. \tag{27}$$

Then, we can obtain the following results by using the MGF:

$$\mathrm{E}\left[e^{-\frac{T^d_i}{4N_0}}\right] = \mathrm{E}\left[e^{-\frac{\sum_{r=1}^{N_r}\sum_{\tilde{u}^i_{at} \in \Omega^d_{ij}} \rho \left\|\mathbf{H}^r\left\langle\tilde{u}^i_{at}\right\rangle\right\|^2}{4N_0}}\right]. \tag{28}$$

$$= \left(1 + \frac{\rho}{4N_0}\right)^{-N_r\left|\Omega^d_{ij}\right|/2} \tag{29}$$

Similarly, $\mathrm{E}[e^{-\frac{T^d_j}{4N_0}}]$ can be attained as

$$\mathrm{E}[e^{-\frac{T^d_j}{4N_0}}] = (1 + \frac{\rho}{4N_0})^{-N_r\left|\Omega^d_{ij}\right|/2}.$$

Then, the $\mathrm{E}[e^{-\frac{T^s_{ij}}{4N_0}}]$ with $\tilde{u}^i_{ta}, \tilde{u}^j_{t'a} \in \Omega^s_{ij}$ can be represented as

$$\mathrm{E}[\exp\left(-\frac{T^s_{ij}}{4N_0}\right)] \tag{30}$$

$$= \mathrm{E}\left[\exp\left(-\frac{1}{4N_0}\sum_{r=1}^{N_r}\sum_{\Omega^s_{ij}} \rho \left\|\mathbf{H}^r\left\langle\tilde{u}^i_{at}\right\rangle - \mathbf{H}^r\left\langle\tilde{u}^j_{at'}\right\rangle\right\|^2\right)\right] \tag{31}$$

$$= \left(1 + \frac{\rho}{2N_0}\right)^{-N_r\left|\Omega^s_{ij}\right|/2}. \tag{32}$$

The components in (26) can be obtained similarly. Hence, the virtual index PEP with $\mathcal{M}$-PSK and $j \in \Lambda_i$ is shown in (33), as shown at the bottom of the next page.

For analyzing the error events related to the virtual APM symbol, we model the ML receiver as an L branch MRC receiver as in [37]. Then, the error probability of a single virtual APM symbol conditioned on the instantaneous channel coefficient matrix $\mathbf{H}$ can be expressed as

$$P_{M|\mathbf{H}} \approx 2Q(\sqrt{\frac{2\sum_{r=1}^{N_r}\sum_{u_{at} \in \mathbf{w}_{ct}} \rho \left\|\mathbf{H}^r\left\langle u_{at}\right\rangle\right\|^2}{N_0}} \sin(\pi/M)). \tag{34}$$

By considering $\mathcal{M}$-PSK and the MGF method, the unconditional error probability can be given as

$$P_M \approx \frac{1}{6}(1 + \frac{\rho}{N_0}\sin^2(\frac{\pi}{M}))^{-dN_r} + \frac{1}{2}(1 + \frac{4}{3N_0}\sin^2(\frac{\pi}{M}))^{-dN_r}. \tag{35}$$

Thus, when the indices of the virutal blocks are detected correctly, the error rate of the APM symbol is $(1 - P_V)P_M$. When the indices of the virtual blocks are detected incorrectly, we only consider the case where a single virtual block is detected by mistake. Therefore, $K_v - 1$ APM symbols have an error rate of P_M and the APM symbol error probability for the virtual block with index detection error is $(M - 1)/M$. Then, the total error probability of all the virtual APM symbols in the first group can be given as

$$P^T_M \approx (1 - P_V)P_M + P_V\frac{(K_v - 1)P_M + (M - 1)/M}{K_v}. \tag{36}$$

Therefore, the block error rate (BLER), defined as the ratio of the number of groups in error to the total transmitted groups, can be given as

$$P_G \approx 1 - (1 - P_V)(1 - P^T_M). \tag{37}$$

2) BINDING RESOURCE UNITS WITH OVERLAP

To address the challenge mentioned in Sec. III-B1 and improve the transmit diversity order without sacrificing SE, the scheme of binding with overlapping basic resource units and constellation rotation, termed as ESFIM-O, is proposed in this section. Investigating the first group with $n_b \times N_t$

space-frequency units as well, the binding with overlap means to construct virtual block set $\mathbf{W} = \{\mathbf{w}_{ct}\}$, where $\mathbf{w}_{ct}$ can be expressed as

$$\mathbf{w}_{ct} = \begin{cases} \{u_{1t}, u_{2t}, \ldots u_{dt}\} & c = 1 \\ \{u_{((c-1)(d-d')+1)t}, \ldots, u_{((c-1)(d-d')+d)t}\} & \text{others} \end{cases}$$

where $d' < d$ is the number of the basic units overlapped and can be represented as

$$d' = \left|\mathbf{w}_{ct} \cap \mathbf{w}_{(c+1)t}\right|. \tag{38}$$

For illustrating it more clearly, assuming $N_t = 2$, $n_b = 4$, $d = 3$, $d' = 2$, the elements in the virtual block set $\mathbf{W} = \{\mathbf{w}_{tc}\}$ can be given as

$$\begin{aligned} \mathbf{w}_{11} &= \{u_{11}, u_{21}, u_{31}\} \\ \mathbf{w}_{21} &= \{u_{21}, u_{31}, u_{41}\} \\ \mathbf{w}_{12} &= \{u_{12}, u_{22}, u_{32}\} \\ \mathbf{w}_{22} &= \{u_{22}, u_{32}, u_{42}\}. \end{aligned} \tag{39}$$

Then, the overlapping basic resource units between the virtual building blocks can be represented as

$$\begin{aligned} \mathbf{w}_{11} \cap \mathbf{w}_{21} &= \{u_{21}, u_{31}\}, \\ \mathbf{w}_{12} \cap \mathbf{w}_{22} &= \{u_{22}, u_{32}\}. \end{aligned} \tag{40}$$

If the overlapping units are modulated with the APM signal from the same constellation, the diversity for the worst case PEP can only reach two. To address this issue, we propose to modulate the virtual blocks with basic resource units overlapped with APM symbols chosen from different constellations. Denote $\mathcal{Q}$ and $\mathcal{Q}'$ as the constellations used to map APM symbols to the virtual block $\mathbf{w}_{ct}$ and $\mathbf{w}_{c't}$, respectively. Then, $\mathcal{Q}$ and $\mathcal{Q}'$ should meet

$$\mathcal{Q} \cap \mathcal{Q}' = \emptyset \quad \text{if } \mathbf{w}_{ct} \cap \mathbf{w}_{c't} \neq \emptyset. \tag{41}$$

Different constellations can be obtained by phase rotation, i.e., $\mathcal{Q}' = \mathcal{Q}e^{j\theta}$, where θ is chosen to maximize the minimum distance of the symbols in $\{\mathcal{Q} \cup \mathcal{Q}'\}$.

Besides the separation in Sec. III-B1, additional set, where same basic resource units are in the virtual blocks represented by the indice $\tilde{v}^i$ and $\tilde{v}^j$, is needed. The set for these basic resource units can be represented as

$$\Omega_{ij}^{ss} = \{\tilde{u}_{at}^i, \tilde{u}_{at}^j\}. \tag{42}$$

Therefore, the instantaneous PEP can be given as

$$P(\Psi^i \to \Psi^j|\mathbf{H}) = Q\left(\sqrt{\frac{T_i^d + T_j^d + T_{ij}^s + T_{ij}^{ss}}{2N_0}}\right). \tag{43}$$

The additional component related to T_{ij}^{ss} can be given in (44), as shown on the bottom of next page, where d_min($\mathcal{Q}$, $\mathcal{Q}'$) is the minimum Euclidean distance of arbitrary symbol pairs in $\mathcal{Q}$ and $\mathcal{Q}'$. And the remaining calculation is identical to the Sec. III-B1.

TABLE 1. Simulation parameters.

Number of transmit antennas	$N_t = 2$
Number of receive antennas	$N_r = 2$
Number of subcarriers	$N = 120$
Number of groups	$G = 30$
Number of paths of channel	$L_h = 8$
Length of CP	$L_{cp} = 8$

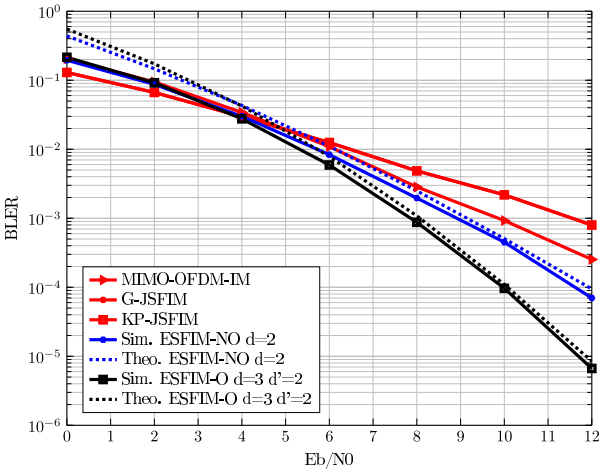

FIGURE 6. BLER comparison among MIMO-OFDM-IM, G-JSFIM, KP-JSFIM, ESFIM-NO, and ESFIM-O with SE = 1.5 bits/s/Hz.

IV. SIMULATIONS

In this section, the numerical results are presented to verify the correctness of the theoretical analysis and system performances. For the followings, the simulation parameters are presented in Table1.

In Fig. 6, the BLER of the proposed ESFIM-NO and ESFIM-O are compared with MIMO-OFDM-IM, G-JSFIM and KP-JSFIM. For the proposed scheme, two out of four virutal blocks are activated for each group consisting of two transmit antennas and four subcarriers and each virtual block is mapped with a QPSK symbol, resulting in a spectral efficiency of 1.5 bits/s/Hz. From the simulation results, the significant performance gains are achieved for ESFIM-NO and ESFIM-O. More specifically, at BLER $= 10^{-3}$, the ESFIM-NO and ESFIM-O have SNR gains of approximately 1 dB and 2 dB over MIMO-OFDM-IM, respectively. The theoretical upper bounds are very tight to the simulation results and the diversities attained by ESFIM-NO and ESFIM-O are clearly shown.

$$P(\Psi^i \to \Psi^j) \approx \frac{1}{12}\left(1 + \frac{\rho}{4N_0}\right)^{-N_r\left|\Omega_{ij}^d\right|}\left(1 + \frac{\rho}{2N_0}\right)^{-N_r\left|\Omega_{ij}^s\right|/2} + \frac{1}{4}\left(1 + \frac{\rho}{3N_0}\right)^{-N_r\left|\Omega_{ij}^d\right|}\left(1 + \frac{2\rho}{3N_0}\right)^{-N_r\left|\Omega_{ij}^s\right|/2} \tag{33}$$

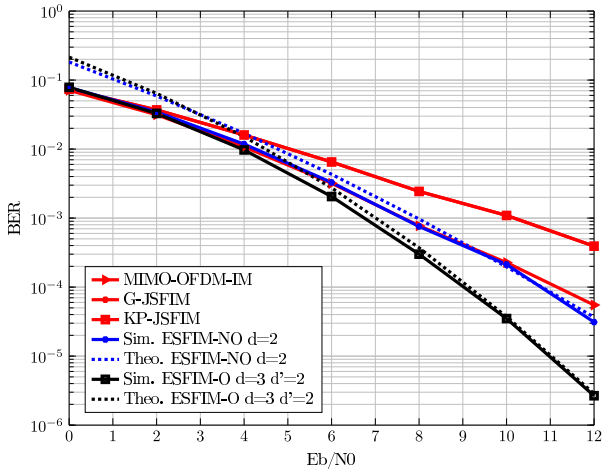

FIGURE 7. BER comparison among MIMO-OFDM-IM, G-JSFIM, KP-JSFIM, ESFIM-N, and ESFIM-O with SE = 1.5 bits/s/Hz.

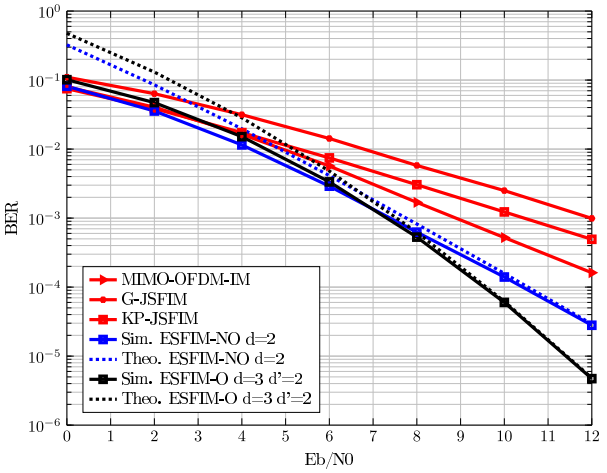

FIGURE 9. BER comparison among MIMO-OFDM-IM, G-JSFIM, KP-JSFIM, ESFIM-NO, and ESFIM-O with SE = 2 bits/s/Hz.

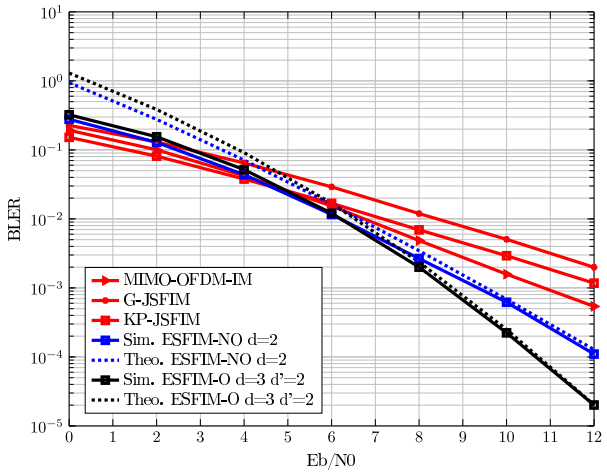

FIGURE 8. BLER comparison among MIMO-OFDM-IM, G-JSFIM, KP-JSFIM, ESFIM-NO, and ESFIM-O with SE = 2 bits/s/Hz.

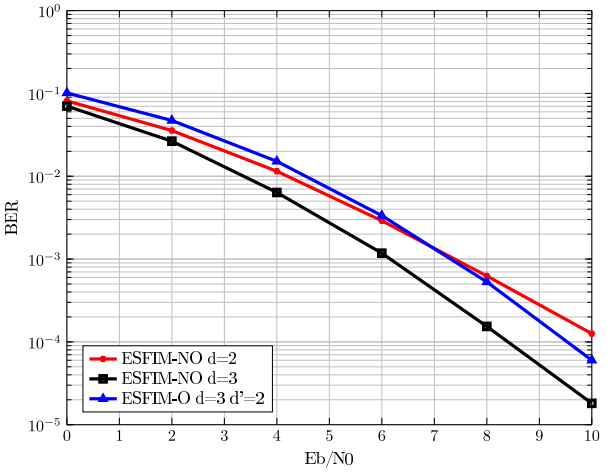

FIGURE 10. BER comparison between ESFIM-NO with $d = 2$, $d = 3$ and ESFIM-O with $d = 3, d' = 2$.

In Fig.7, the BER performance of ESFIM-NO, and ESFIM-O are compared with MIMO-OFDM-IM, G-JSFIM and KP-JSFIM at SE= 1.5 bits/s/Hz. We show that the BER performance of ESFIM-NO with $d = 2$ and MIMO-OFDM-IM are close. Meanwhile, ESFIM-O shows its superior performance due to high transmit diversity order of three. At the BER of 10^{-4}, ESFIM-O can harvest an SNR gain of approximately 3 dB compared to MIMO-OFDM-IM.

The similar comparisons are carried out for SE= 2 bits/s/Hz, where three virutal blocks are selected from a group with four virtual blocks and each block is mapped with a QPSK symbol.The BLER and BER performance results are shown in Fig. 8 and Fig. 9. As shown in Fig. 8, the performance gain for ESFIM-NO and ESFIM-O are significant. More specifically, at BLER of 10^{-3}, ESFIM-NO and ESFIM-O can achieve approximately 1.5 dB and 2 dB SNR gains over conventional MIMO-OFDM-IM,

$$\mathrm{E}\left[\exp\left(-\frac{T_{ij}^{ss}}{4N_0}\right)\right] = \mathrm{E}\left[\exp\left(-\frac{1}{4N_0}\sum_{r=1}^{N_r}\sum_{\tilde{u}_{at}^{i},\tilde{u}_{at}^{j}\in\Omega_{ij}^{ss}}\rho\left\|\mathbf{H}^{r}\left\langle\tilde{u}_{at}^{i}\right\rangle\right\|^{2}\left\|\mathbf{S}^{i}\left\langle\tilde{u}_{at}^{i}\right\rangle-\mathbf{S}^{j}\left\langle\tilde{u}_{at}^{j}\right\rangle\right\|^{2}\right)\right]$$
$$< \left(1+\frac{\rho}{4N_0}\left(\mathrm{d\_min}(\mathcal{Q},\mathcal{Q}')\right)^{2}\right)^{-N_r\left|\Omega_{ij}^{ss}\right|} \tag{44}$$

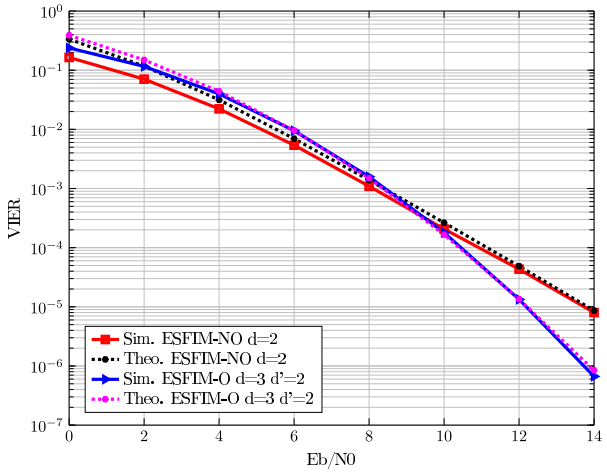

FIGURE 11. Comparison of VIER for ESFIM-NO and ESFIM-O.

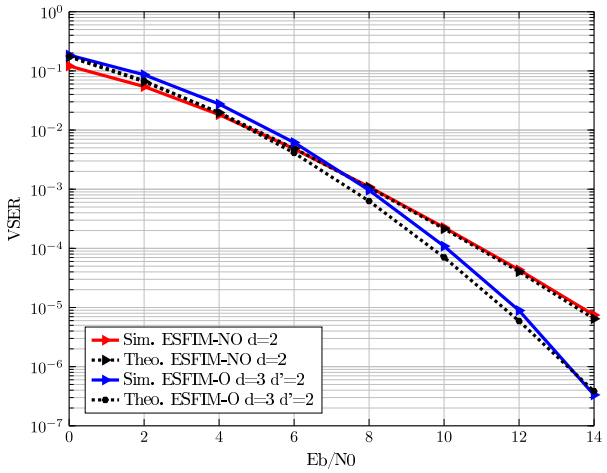

FIGURE 12. Comparison of VSER for ESFIM-NO and ESFIM-O.

respectively. In Fig. 9, the performance improvements are more evident compared to the results shown in Fig 7.

In Fig.10, the BER of ESFIM-NO with $d = 2$ and $d = 3$ and ESFIM-O with $d = 3$ $d' = 2$ are compared, where ESFIM-NO with $d = 2$ and ESFIM-O with $d = 3$ can reach spectrum efficiency of 2 bits/s/Hz, while ESFIM-NO with $d = 3$ can only reach SE= 1.33bits/s/Hz. As shown in the figure, ESFIM-O with $d = 3$ outperforms ESFIM-NO with $d = 2$ for high SNR due to its transmit diversity advantages. However, at low SNR range, the BER performance of ESFIM-NO with $d = 2$ is slightly better than ESFIM-O with $d = 3$. This is because that the minimum Euclidean distance of the constellation determine the BER performance in low SNR, and ESFIM-NO with $d = 2$ has larger minimum Euclidean distance than ESFIM-O with $d = 3$. In addition to the high diversity, the ESFIM-NO with $d = 3$ has the largest minimum Euclidean distance, therefore it outperforms ESFIM-NO with $d = 2$ and ESFIM-O with $d = 3$ at the cost of lower spectrum efficiency. From the above results, it can be concluded that space-frequency index modulation provides more flexibility for system designs.

In order to evaluate the diversity of virtual index and APM symbol domains, respectively, the simulation results of VIER and virtual symbol error rate (VSER) are depicted in Fig. 11 and Fig. 12 along with the derived theoretical bounds. It is obvious that ESFIM-O can achieve better diversity than ESFIM-NO in terms of both VIER and VSER. However, ESFIM-NO has slightly better performance than ESFIM-O in the low SNR region. This is because of the usage of different constellations in ESFIM-O, which reduces the minimum Euclidean distance of the combined signal on the overlapping resource units. Again, the spatial-frequency index modulation system provides us with more design freedom to meet the target requirements of HetNets.

V. CONCLUSION

In this paper, a novel framework to design waveforms for one tier of HetNets is investigated. By appropriate binding resources in both spatial and frequency domains to form IM symbols, two novel schemes, termed as ESFIM-NO and ESFIM-O, are proposed. The theoretical and simulation results verify that the proposed two methods can outperform the existing index modulation using spatial and frequency resources in terms of BLER and BER due to its enhanced diversity. More importantly, the analysis and simulation results also show that the space-frequency index modulation system can provide more flexibility to make a balanced tradeoff between system throughput and robustness. However, the complexity of the ML detector is still extremely high, especially for the applications in high date rate transmission. Therefore, developing novel detectors with low complexity is our future research work.

REFERENCES

[1] J. G. Andrews, H. Claussen, M. Dohler, S. Rangan, and M. C. Reed, "Femtocells: Past, present, and future," *IEEE J. Sel. Areas Commun.*, vol. 30, no. 3, pp. 497–508, Apr. 2012.

[2] J. G. Andrews, S. Buzzi, W. Choi, S. V. Hanly, A. Lozano, A. C. K. Soong, and J. C. Zhang, "What will 5G Be?" *IEEE J. Sel. Areas Commun.*, vol. 32, no. 6, pp. 1065–1082, Jun. 2014.

[3] N. Wang, E. Hossain, and V. K. Bhargava, "Joint downlink cell association and bandwidth allocation for wireless backhauling in two-tier HetNets with large-scale antenna arrays," *IEEE Trans. Wireless Commun.*, vol. 15, no. 5, pp. 3251–3268, May 2016.

[4] J. Tang, D. K. C. So, E. Alsusa, K. A. Hamdi, and A. Shojaeifard, "Resource allocation for energy efficiency optimization in heterogeneous networks," *IEEE J. Sel. Areas Commun.*, vol. 33, no. 10, pp. 2104–2117, Oct. 2015.

[5] S. Cai, Y. Che, L. Duan, J. Wang, S. Zhou, and R. Zhang, "Green 5G heterogeneous networks through dynamic small-cell operation," *IEEE J. Sel. Areas Commun.*, vol. 34, no. 5, pp. 1103–1115, May 2016.

[6] M. Agiwal, A. Roy, and N. Saxena, "Next generation 5G wireless networks: A comprehensive survey," *IEEE Commun. Surveys Tuts.*, vol. 18, no. 3, pp. 1617–1655, 3rd Quart., 2016.

[7] H. S. Dhillon, M. Kountouris, and J. G. Andrews, "Downlink MIMO HetNets: Modeling, ordering results and performance analysis," *IEEE Trans. Wireless Commun.*, vol. 12, no. 10, pp. 5208–5222, Oct. 2013.

[8] L. Sanguinetti, A. L. Moustakas, and M. Debbah, "Interference management in 5G reverse TDD HetNets with wireless backhaul: A large system analysis," *IEEE J. Sel. Areas Commun.*, vol. 33, no. 6, pp. 1187–1200, Jun. 2015.

[9] A. Nasser, O. Muta, M. Elsabrouty, and H. Gacanin, "Interference mitigation and power allocation scheme for downlink MIMO–NOMA HetNet," *IEEE Trans. Veh. Technol.*, vol. 68, no. 7, pp. 6805–6816, Jul. 2019.
[10] Y. Dhungana and C. Tellambura, "Performance analysis of SDMA with inter-tier interference nulling in HetNets," *IEEE Trans. Wireless Commun.*, vol. 16, no. 4, pp. 2153–2167, Apr. 2017.
[11] Y. Liu, Z. Qin, M. Elkashlan, A. Nallanathan, and J. A. Mccann, "Non-orthogonal multiple access in large-scale heterogeneous networks," *IEEE J. Sel. Areas Commun.*, vol. 35, no. 12, pp. 2667–2680, Dec. 2017.
[12] B. Xu, Y. Chen, J. R. Carrion, and T. Zhang, "Resource allocation in energy-cooperation enabled two-tier NOMA HetNets toward green 5G," *IEEE J. Sel. Areas Commun.*, vol. 35, no. 12, pp. 2758–2770, Dec. 2017.
[13] J. Zhao, Y. Liu, K. K. Chai, A. Nallanathan, Y. Chen, and Z. Han, "Spectrum allocation and power control for non-orthogonal multiple access in HetNets," *IEEE Trans. Wireless Commun.*, vol. 16, no. 9, pp. 5825–5837, Sep. 2017.
[14] S. Dogan, A. Tusha, and H. Arslan, "NOMA with index modulation for uplink URLLC through grant-free access," *IEEE J. Sel. Topics Signal Process.*, vol. 13, no. 6, pp. 1249–1257, Oct. 2019.
[15] E. Basar, "Index modulation techniques for 5G wireless networks," *IEEE Commun. Mag.*, vol. 54, no. 7, pp. 168–175, Jul. 2016.
[16] N. Ishikawa, S. Sugiura, and L. Hanzo, "50 years of permutation, spatial and index modulation: From classic RF to visible light communications and data storage," *IEEE Commun. Surveys Tuts.*, vol. 20, no. 3, pp. 1905–1938, 3rd Quart., 2018.
[17] S. Sugiura, T. Ishihara, and M. Nakao, "State-of-the-art design of index modulation in the space, time, and frequency domains: Benefits and fundamental limitations," *IEEE Access*, vol. 5, pp. 21774–21790, 2017.
[18] T. Mao, Q. Wang, Z. Wang, and S. Chen, "Novel index modulation techniques: A survey," *IEEE Commun. Surveys Tuts.*, vol. 21, no. 1, pp. 315–348, 1st Quart., 2018.
[19] Y. A. Chau and S.-H. Yu, "Space modulation on wireless fading channels," in *Proc. IEEE Veh. Technol. Conf. VTC Fall*, Atlantic City, NJ, USA, vol. 3, Oct. 2001, pp. 1668–1671.
[20] E. Basar, "Orthogonal frequency division multiplexing with index modulation," *IEEE Trans. Signal Process.*, vol. 61, no. 22, pp. 5536–5549, Nov. 2013.
[21] M. I. Kadir, "Generalized space-time-frequency index modulation," *IEEE Commun. Lett.*, vol. 23, no. 2, pp. 250–253, Feb. 2019.
[22] E. Basar, M. Wen, R. Mesleh, M. Di Renzo, Y. Xiao, and H. Haas, "Index modulation techniques for next-generation wireless networks," *IEEE Access*, vol. 5, pp. 16693–16746, 2017.
[23] P. Yang, M. Di Renzo, Y. Xiao, S. Li, and L. Hanzo, "Design guidelines for spatial modulation," *IEEE Commun. Surveys Tuts.*, vol. 17, no. 1, pp. 6–26, 1st Quart., 2015.
[24] M. Di Renzo, H. Haas, A. Ghrayeb, S. Sugiura, and L. Hanzo, "Spatial modulation for generalized MIMO: Challenges, opportunities, and implementation," *Proc. IEEE*, vol. 102, no. 1, pp. 56–103, Jan. 2014.
[25] Y. Xiao, S. Wang, L. Dan, X. Lei, P. Yang, and W. Xiang, "OFDM with interleaved subcarrier-index modulation," *IEEE Commun. Lett.*, vol. 18, no. 8, pp. 1447–1450, Aug. 2014.
[26] E. Basar, "OFDM with index modulation using coordinate interleaving," *IEEE Wireless Commun. Lett.*, vol. 4, no. 4, pp. 381–384, Aug. 2015.
[27] J. Zheng and R. Chen, "Achieving transmit diversity in OFDM-IM by utilizing multiple signal constellations," *IEEE Access*, vol. 5, pp. 8978–8988, 2017.
[28] T. V. Luong, Y. Ko, and J. Choi, "Repeated MCIK-OFDM with enhanced transmit diversity under CSI uncertainty," *IEEE Trans. Wireless Commun.*, vol. 17, no. 6, pp. 4079–4088, Jun. 2018.
[29] E. Basar, "Multiple-input multiple-output OFDM with index modulation," *IEEE Signal Process. Lett.*, vol. 22, no. 12, pp. 2259–2263, Dec. 2015.
[30] R. Chen and J. Zheng, "Index-Modulated MIMO-OFDM: Joint space-frequency signal design and linear precoding in rapidly time-varying channels," *IEEE Trans. Wireless Commun.*, vol. 17, no. 10, pp. 7067–7079, Oct. 2018.
[31] T. Datta, H. S. Eshwaraiah, and A. Chockalingam, "Generalized space-and-frequency index modulation," *IEEE Trans. Veh. Technol.*, vol. 65, no. 7, pp. 4911–4924, Jul. 2016.
[32] D. Singh and H. D. Joshi, "Performance analysis of SFBC-OFDM system with channel estimation error over generalized fading channels," *Trans. Emerg. Telecommun. Technol.*, vol. 29, no. 3, p. e3293, Mar. 2018.
[33] D. Singh and H. D. Joshi, "BER performance of SFBC OFDM system over TWDP fading channel," *IEEE Commun. Lett.*, vol. 20, no. 12, pp. 2426–2429, Dec. 2016.
[34] S. Lu, I. A. Hemadeh, M. El-Hajjar, and L. Hanzo, "Compressed sensing-aided multi-dimensional index modulation," *IEEE Trans. Commun.*, vol. 67, no. 6, pp. 4074–4087, Jun. 2019.
[35] M. Wen, X. Chen, Q. Li, E. Basar, Y.-C. Wu, and W. Zhang, "Index modulation aided subcarrier mapping for dual-hop OFDM relaying," *IEEE Trans. Commun.*, vol. 67, no. 9, pp. 6012–6024, Sep. 2019.
[36] S. Dang, J. Li, M. Wen, S. Mumtaz, and Z. Zhang, "OFDM-IM based dual-hop system using fixed-gain amplify-and-forward relay with pre-processing capability," *IEEE Trans. Wireless Commun.*, vol. 18, no. 4, pp. 2259–2270, Apr. 2019.
[37] M.-S. Alouini and A. J. Goldsmith, "A unified approach for calculating error rates of linearly modulated signals over generalized fading channels," *IEEE Trans. Commun.*, vol. 47, no. 9, pp. 1324–1334, Sep. 1999.

RUI CAO received the B.S. and M.S. degrees from the University of Electronic Science and Technology of China (UESTC), in 2005 and 2008, respectively, where he is currently pursuing the Ph.D. degree with the National Key Laboratory of Science and Technology on Communications. His main research interests include index modulation systems, and precoding and performance analysis of wireless communications.

XIA LEI received the Ph.D. degree in communication and information systems from the University of Electronic Science and Technology of China, Chengdu, China, in 2005. She is currently a Professor and a Supervisor of Ph.D. degree candidates with the University of Electronic Science and Technology of China. She has published more than 60 international journals. Her major research interests include mobile communication, multicarrier techniques, and cooperative wireless communications.

YUE XIAO (Member, IEEE) received the Ph.D. degree in communication and information systems from the University of Electronic Science and Technology of China (UESTC), in 2007. He is currently a Professor with the National Key Laboratory of Science and Technology on Communications, UESTC. He has published more than 100 international journals and has been the in charge of more than 20 projects in the areas of Chinese 3G/4G/5G wireless communication systems. He is an inventor of more than 50 Chinese and PCT patents on wireless systems. His research interest includes system design and signal processing toward future wireless communication systems. He currently serves as an Associate Editor of the IEEE COMMUNICATIONS LETTERS.

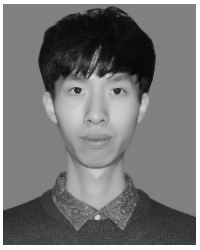

YOU LI received the B.S. degree in communication and information systems from the University of Electronic Science and Technology of China (UESTC), in 2013, where he is currently pursuing the Ph.D. degree with the National Key Laboratory of Science and Technology on Communications. His research interest includes spatial modulation toward future wireless communication systems.